Anisotropic rheology during grain boundary diffusion creep and its relation to grain rotation, grain boundary sliding and superplasticity

John Wheeler

Anisotropic rheology during grain boundary diffusion creep and its relation to grain rotation, grain boundary sliding and superplasticity

Journal:	*Philosophical Magazine & Philosophical Magazine Letters*
Manuscript ID:	TPHM-09-Oct-0428
Journal Selection:	Philosophical Magazine
Date Submitted by the Author:	15-Oct-2009
Complete List of Authors:	Wheeler, John; Liverpool University, Earth and Ocean Sciences
Keywords:	creep, deformation mechanisms, mechanics of materials, grain boundary diffusion, microstructure, superplastic deformation
Keywords (user supplied):	

Anisotropic rheology during grain boundary diffusion creep and its relation to grain rotation, grain boundary sliding and superplasticity

J. WHEELER

Dept. Earth and Ocean Sciences, Liverpool University, Liverpool L69 3GP, U.K.
johnwh@liv.ac.uk

The response of periodic microstructures to deformation can be analysed rigorously and this provides guidance in understanding more complex microstructures. When deforming by diffusion creep accompanied by sliding, irregular hexagons are shown to be anisotropic in their rheology. Analytic solutions are derived in which grain rotation is a key aspect of the deformation. If grain boundaries cannot support shear stress, the polycrystal viscosity is extremely anisotropic. There are two orthogonal directions of zero strength: sliding and rotation cooperate to allow strain parallel to these directions to be accomplished without any dissolution or plating. When a linear velocity/shear stress relationship is introduced for grain boundaries, the anisotropy is less extreme, but two weak directions still exist along which polycrystal strength is controlled only by the grain boundary "viscosity". Irregular hexagons are characterised by 4 parameters. A particular subset of hexagons defined by 2 parameters, which includes regular hexagons as well as some elongate shapes, shows singular behaviour. Grain shapes that are close to that of the subset may exhibit large grain rotation rates and have no well-defined rheology unless there is a finite grain boundary viscosity. This new analysis explains why microstructures based on irregular but near equi-axed grains show high rotation rates during diffusion creep and it provides a framework for understanding strength anisotropy during diffusion creep.

1. Introduction

In crystalline materials, grain boundary diffusion creep (Coble creep in metals and ceramics, or solution-aided mass transfer in rocks) is an important deformation mechanism [1-3]. It plays a role in superplastic behaviour of metals, and is important in how the Earth deforms on long timescales [4]. It is established that grain boundary sliding must accompany diffusion to maintain compatibility between grains [5, 6].

Grain rotations are an integral aspect of diffusion creep [7]. They are particularly important as they are commonly cited as the reason (at least in part) why grains remain quite equi-axed at high strains during superplastic deformation. In

geology grain rotations are important for that reason and more. In rocks there is commonly a lattice preferred orientation (LPO) which gives rise to elastic anisotropy and hence anisotropy in seismic wave velocities. Thus LPO can be detected deep in the Earth via monitoring seismic waves. Grain rotations during diffusion creep can in principle destroy seismic anisotropy by rotating different grains in different ways. This has been postulated as a mechanism for destroying LPO but critical experiments are lacking. Wheeler [8] gave a numerical model for rotations during diffusion creep and shows that they may be limited in extent under particular imposed deformations. Consequently grain rotations should be the focus of further research.

The flow law for diffusion creep shows that strain rate is proportional to stress, and grain size has a major effect: for Coble creep strain rate is proportional to the inverse cube of grain size. Much less has been said about the possible anisotropy of rheology, although it is predicted to occur [9, 10]. Anisotropy may be the result of elongate grain shapes, which mean diffusion path lengths are different in different directions. Anisotropy is important because it can give rise to strain localisation. For example, envisage an anisotropic polycrystal with local areas in "soft" orientations relative to an imposed shear stress. These soft orientations will focus strain which, depending on the link between microstructure and rheology, may evolve to be yet weaker and hence localise strain further.

Numerical models of diffusion creep encompass polycrystals with irregular grain shapes [2, 11] and include the combined operation of stress-induced diffusion, grain rotation, and grain boundary sliding, sometimes with a shear stress term [12], and the effects of different imposed deformations (pure and simple shear etc.) [8]. In general, the behaviour of a large complex array of grains must be dealt with by numerical modelling. Grain-scale analytic studies can address only simple microstructures, but provide more insight into the reasons for particular behaviours. Examples include parallelepipeds [9], regular hexagons [5], cubes [13], orthorhombic shapes [10], cylinders [6], elongate hexagons with a mirror plane [12], and regular hexagons in shear [14].

In this contribution I present the analytic solution for the rheology and grain-rotation behaviour of a periodic microstructure made of one grain shape (an irregular hexagon). There are 4 motivations for this study.

1. An analytic solution for a regular microstructure can provide a basis for understanding behaviour of irregular microstructures (which can be regarded in a

general fashion as “perturbed” regular microstructures). In particular numerical simulations of irregular microstructures show that relative grain rotations are much larger when grains are equi-axed than when they are elongate [8]: the analysis here will show why that is the case.

2. There are various separate treatments of hexagonal microstructures with different imposed deformations in the literature and it is not clear how these analyses link together to form a coherent whole: the full 2D solution for arbitrary hexagonal shapes and general deformations has never been presented. As I will show, the full theory provides substantial new insight.

3. The analytic solution provides a framework for understanding rheological anisotropy as a function of grain shape, and the effects on rheology of shear stress along grain boundaries.

4. The analytic solution provides a test for the correctness of numerical methods.

I begin the next section with a kinematic analysis: I show how an imposed strain rate field will relate to local grain rotations, dissolution/precipitation rates and sliding rates along boundaries in a periodic microstructure. This is followed by deriving the general equations for force balance, which are applied to diffusion creep with and without shear stress on grain boundaries. I then show how these equations are solved (for any grain shape and any imposed deformation rate) to derive the angular velocity of grains, the stress, and the viscosity tensor for the polycrystal. Specific grain shapes, or families of shapes defined by one parameter, are used to illustrate the general predictions. Finally I discuss the general significance of this work in understanding diffusion creep.

2. Periodic microstructure: geometry and kinematics

In this section I establish the basic description of the hexagonal tessellation and show how an imposed deformation rate tensor can, together with a specified angular velocity, be used to predict growth/dissolution rates along each grain boundary. Figure 1 shows a microstructure made by tessellating a single grain shape, that of an irregular hexagon. Each hexagon has 3 pairs of parallel faces, denoted by vectors $\mathbf{B}_i$. These are linked by vectors $\mathbf{R}_i$ defining the translational symmetry of the tessellation. The choice of vectors is made so that the actual shape is the same if there

is a cyclic interchange of the three boundary vectors (123 → 312 etc.), which is advantageous for analysis since it implies that many equations should be invariant under such cyclic interchanges.

It can be seen that:

$$\boldsymbol{R}_1 = \boldsymbol{B}_2 @ \boldsymbol{B}_3$$
$$\boldsymbol{R}_2 = \boldsymbol{B}_3 @ \boldsymbol{B}_1 \qquad (1)$$
$$\boldsymbol{R}_3 = \boldsymbol{B}_1 @ \boldsymbol{B}_2$$

There are 2 distinct types of triple junction in this microstructure, TJ_a and TJ_b which are not related to each other by translational symmetry.

Suppose that a deformation rate **D**, homogeneous on the large scale, is imposed on this microstructure. Deformation at the scale of one grain will be accomplished by dissolution, precipitation and sliding at grain boundaries, with no internal strain in the grain, but possibly with rotation of the grain. In general the movement of each grain is characterised by a velocity **w** at the origin and an angular velocity ω (positive anticlockwise) [2], so that the velocity of any point **x** in that grain is given by:

$$\boldsymbol{v} = \boldsymbol{w} + \omega \boldsymbol{S} \boldsymbol{x} \qquad (2)$$

where **S** is the skew tensor

$$\boldsymbol{S} = \begin{matrix} \text{“} & @1\text{”} \\ 1 & 0 \end{matrix} \qquad (3)$$

Although the behaviour at grain scale is heterogeneous, consider different grains G1 and G2. It is to be expected that any two points $\mathbf{x}_{G1}$ and $\mathbf{x}_{G2}$ related by a translational symmetry vector **R** will have velocities related by

$$\boldsymbol{v}_{G2} @ \boldsymbol{v}_{G1} = \boldsymbol{D}\boldsymbol{R} \qquad (4)$$

If there is any rotation, there must be a single value of angular velocity for all grains. So when two grains are related by **R** we must have

$$\boldsymbol{w}_{G2} + \omega \boldsymbol{S} \quad \boldsymbol{x} + \boldsymbol{R}^{\text{“}} @ \boldsymbol{w}_{G1} @ \omega \boldsymbol{S} \boldsymbol{x} = \boldsymbol{D}\boldsymbol{R}$$

so

$$\boldsymbol{w}_{G2} @ \boldsymbol{w}_{G1} = \boldsymbol{D} @ \omega \boldsymbol{S}^{\text{“}} \boldsymbol{R}$$

The important kinematic quantity is the relative velocity of two grains at their contact. Using Eq. (2) for grains G1 and G2 but with the *same* value of **x** we find that, regardless of the boundary position,

$$\Delta \boldsymbol{v} = \boldsymbol{w}_{G2} + \omega \boldsymbol{S}\,\boldsymbol{x} - \boldsymbol{w}_{G1} - \omega \boldsymbol{S}\boldsymbol{x} = \boldsymbol{D} - \omega \boldsymbol{S}^{\perp}\boldsymbol{R} \tag{5}$$

This can be split into normal and transverse relative velocities for each boundary *i*, using the unit vector $\mathbf{N}_i$ normal to the boundary and unit vector $\mathbf{T}_i$ parallel to it, with the signs being governed by the "anticlockwise" construction of the vectors $\mathbf{B}_i$ (Fig. 1).

$$u_i = \boldsymbol{N}_i \cdot \boldsymbol{D} - \omega \boldsymbol{S}^{\perp}\boldsymbol{R}_i \tag{6}$$

(positive indicates moving apart of the two grains) and

$$t_i = \boldsymbol{T}_i \cdot \boldsymbol{D} - \omega \boldsymbol{S}^{\perp}\boldsymbol{R}_i \tag{7}$$

(positive indicates clockwise or dextral shear component along boundary). Note that if a deformation rate is imposed, the angular velocity is the only unknown kinematic variable.

3. Force balance

For this regular tessellation there are some relationships between the local forces on grain boundaries and the average (macroscopic) stress which prove useful later. It is assumed that the material deforms slowly, so there are no accelerations or angular accelerations. This means that there is no net force and no net moment on any grain [2]. Let $\mathbf{F}_i$ be the net force along boundary *i* pointing *into* the grain. Then, by translational symmetry and force balance, the boundary opposite to *i* has force $-\mathbf{F}_i$ acting on it. Thus, force balance is assured. Suppose we have some arbitrarily complicated traction distribution along each grain boundary i, specified by $\mathbf{f}_i(s)$ acting *outwards* from the grain, where s is distance along the boundary. The moment due to this is given by

$$\int_0^{a} \boldsymbol{f}(s) \times \boldsymbol{x}\, ds \tag{8}$$

where the 2D cross product (a scalar) is indicated

$$\boldsymbol{a} \times \boldsymbol{b} = a_x b_y - a_y b_x = \boldsymbol{b} \cdot \boldsymbol{S}\boldsymbol{a} \tag{9}$$

Because of translational symmetry, the force distribution on one member of the pair must be the opposite of that on the other. So the contribution of a pair of boundaries to the moment is

$$\int_{2\,bdys} \boldsymbol{f}\,ds \times \boldsymbol{x}\,ds = \int \boldsymbol{f}\,ds \times \boldsymbol{x}\,ds + \int @\boldsymbol{f}\,ds \times \boldsymbol{x} + \boldsymbol{R}\,ds = \int @\boldsymbol{f}\,ds \times \boldsymbol{R}\,ds = \boldsymbol{F} \times \boldsymbol{R} \tag{10}$$

where **F** is defined as the net force on the boundary, pointing *into* the grain. The net moment on the grain is obtained by summing over the 3 pairs of boundaries:

$$0 = \sum_{i=1}^{3} \boldsymbol{F}_i \times \boldsymbol{R}_i \tag{11}$$

What is the average value of the stress, which could be used to describe the large-scale behaviour of the material as if it were homogeneous? We take compressive stresses as positive. It is known that the average value of stress within a region can be written in terms of forces f_α at the boundary of the region, regardless of the complexity of stress within that region [15, 16 p. 389] in 3D

$$\int \sigma_{\alpha\beta}\,dV = \int f_\alpha\, x_\beta\, dS$$

where dV is a volume element and dS a surface area element, and in 2D

$$\int \sigma_{\alpha\beta}\,dA = \int f_\alpha\, x_\beta\, ds$$

where dA is an area element and ds is a boundary length element, or, where $\otimes$ indicates the outer (tensor) product of two vectors,

$$\int \sigma\,dA = \int \boldsymbol{f} \otimes \boldsymbol{x}\,ds \tag{12}$$

f is the force resolved along an outwards-facing normal. Let the 2D region under consideration be one grain. Then the boundary consists of three pairs of parallel faces. Because of translational symmetry, the force distribution on one member of the pair must be the opposite of that on the other. So

$$\int_{2\,bdys} \boldsymbol{f} \otimes \boldsymbol{x}\, ds = \int \boldsymbol{f}\, s \otimes \boldsymbol{x}\, ds + \int \boldsymbol{f}\, s \otimes \dot{\boldsymbol{x}} + \boldsymbol{R}\, ds = \int \boldsymbol{f}\, s \otimes \boldsymbol{R}\, ds = \boldsymbol{F} \otimes \boldsymbol{R}$$

Hence the average stress in the grain is obtained by summing over the 3 pairs of boundaries (see also [17]):

$$\sigma = \frac{1}{A} \sum_{i=1}^{3} \boldsymbol{F}_i \otimes \boldsymbol{R}_i \qquad (13)$$

The stress tensor must be symmetric, but this is assured as a consequence of Eq. (11), noting that **a**⊗**b** is a symmetric tensor iff **a** × **b** = 0.

4. Equations for grain boundary diffusion

The previous two sections are quite general insofar as they make no assumptions about the details of stress distributions. The aim in this section is to show how precipitation rates (velocity differences at grain boundaries) in grain boundary diffusion creep relate to forces on the boundaries. Diffusion is driven by gradients in chemical potential (in metals, these are linked to gradients in vacancy concentration) which, in diffusion creep, are in turn related to gradients in normal stress at interfaces: for details see Ford et al. [2]. The diffusive current along a boundary is given by

$$C = -LVw \frac{\partial}{\partial s} \qquad (14)$$

where L is the Onsager diffusion coefficient, w is the effective grain boundary width, and V the molar volume and C is current in mol/m/s. σ_n is the component of stress normal to the boundary (compressive positive). The Onsager coefficient is used so that the same mathematical framework can apply to diffusion of vacancies (as in metals) or of ionic species dissolved in an aqueous grain boundary film (as in rocks), compare for example Cocks et al. [18] eqn. 2.4. If grains move apart at velocity u, mass balance together with Eq. (14) dictates that

$$u = -V \frac{\partial \sigma}{\partial s} = LV^2 w \frac{\partial^2}{\partial s^2} \qquad (15)$$

For convenience we define $Z = LV^2w$. In a complicated microstructure, grains can rotate relative to each other in which case u is a linear function of s and σ_n is cubic in s. However, in the microstructure discussed here, there are no differential rotations and σ_n is quadratic. Consequently we can integrate (15) to obtain

$$\sigma_n(s) = \frac{\sigma_s + \sigma_e}{2} + \frac{u B^2}{8Z} + \frac{\sigma_e - \sigma_s}{B} s + \frac{u}{2Z} s^2 \qquad (16)$$

where σ_s and σ_e are the normal stress values at the start and end of the boundary, B is the boundary length and s is distance along the boundary with the centre point as origin (so it runs from –B/2 to B/2). The current is then

$$C = \frac{Z}{V}\left(\frac{\sigma_e - \sigma_s}{B}\right) + \frac{u}{V} s \qquad (17)$$

There are only two types of node which are not related by symmetry, labelled TJ_a and TJ_b on Fig. 1. There are thus two (unknown) values of normal stress at nodes, which we define as σ_a and σ_b. Writing out Eq. (17) for each boundary we have, for normal stresses and currents:

$$C_1(s) = \frac{Z}{V}\left(\frac{\sigma_b - \sigma_a}{B_1}\right) + \frac{u_1}{V} s$$

$$C_2(s) = \frac{Z}{V}\left(\frac{\sigma_a - \sigma_b}{B_2}\right) + \frac{u_2}{V} s$$

$$C_3(s) = \frac{Z}{V}\left(\frac{\sigma_a - \sigma_b}{B_3}\right) + \frac{u_3}{V} s$$

The net current out of a triple junction should be zero, so for TJ_a, noting that it is at the start point of each of the three boundary vectors,

$$C_1\left(\frac{B_1}{2}\right) + C_2\left(\frac{B_2}{2}\right) + C_3\left(\frac{B_3}{2}\right) = 0$$

Similarly for TJ_b,

$$C_1\left(\frac{B_1}{2}\right) - C_2\left(\frac{B_2}{2}\right) - C_3\left(\frac{B_3}{2}\right) = 0$$

These two equations can be expanded and rearranged to show that

$$\sigma_a = \sigma_b \qquad (18)$$

and

$$u_1 B_1 + u_2 B_2 + u_3 B_3 = 0 \qquad (19)$$

The latter confirms that precipitation rates weighted by boundary length sum to zero as expected since mass is conserved. From previous sections we see that only the net force on a boundary is relevant for the evaluation of moment and average stress. For a generic boundary, the orthogonal force is, from Eq. (16)

$$F^{?} = Z_{-\frac{B}{2}}^{\frac{B}{2}} \sigma_n \, s^{a} ds = \frac{\sigma}{2} B - \frac{1}{12Z} B = \sigma_a B - \frac{1}{12Z} B^3$$

so for each of the 3 boundaries

$$F_i^{?} = \sigma_a B_i - \frac{1}{12Z} B_i^3 \qquad (20)$$

Notice that σ_a contributes in proportion to the length of the boundary and has the character of a pressure. The isotropic component of imposed stress cannot be determined from the imposed deformation rate. Later in this contribution the calculated stress will be adjusted to have zero trace. For this reason, the value of σ_a is irrelevant – it will cancel out in the adjustment – so from now on it is set to zero.

5. Equations for grain boundary sliding

It is common to assign zero shear strength to grain boundaries as part of diffusion creep models, but there is no loss of generalisation by assigning a viscosity as done for example by [9, 19]. It is assumed here that there exists a material constant ζ which relates shear stress to sliding velocity

$$\tau_i = \zeta t_i$$

There is experimental evidence for a linear relationship at least for some temperatures and timescales [20]. Multiplying by the boundary length gives:

$$F_i^{||} = \zeta t_i B_i \qquad (21)$$

If $t_i > 0$, we have dextral movement along the boundary; but then the contribution of $F_i^{||}$ to the force on the grain is in the direction of minus $\mathbf{T}_i$ (Fig. 1). We now have equations which give the forces on the boundaries in terms of the tangential and normal components of relative velocities at each boundary, which are in turn related to the deformation rate tensor and the angular velocity by Eq. (5).

6. Solution of equations

The aim here is to derive expressions for the angular velocity of grain rotation and for anisotropic rheology, the two key concepts discussed in this contribution.

6.1. Angular velocity

The only unknown quantity in this analysis is the angular velocity, and the only constraint not automatically satisfied is that of zero moment (11). We therefore have one equation in one unknown. Combining Eqs. (6), (7), (20) and (21) the force vector on boundary i is

$$\boldsymbol{F}_i = \left(\frac{\pi a^3}{12Z}\boldsymbol{N}_i\cdot\boldsymbol{D} - \omega\boldsymbol{S}\cdot\boldsymbol{R}_i\right)\boldsymbol{N}_i + \left(\zeta B_i\boldsymbol{T}_i\cdot\boldsymbol{D} - \omega\boldsymbol{S}\cdot\boldsymbol{R}_i\right)\boldsymbol{T}_i \qquad (22)$$

Each boundary pair contributes $\boldsymbol{F}_i \times \boldsymbol{R}_i$ to the moment. Noting that

$$\boldsymbol{N}\times\boldsymbol{R} = -\boldsymbol{T}\cdot\boldsymbol{R}$$

and

$$\boldsymbol{T}\times\boldsymbol{R} = \boldsymbol{N}\cdot\boldsymbol{R}$$

we rewrite Eq. (11) as

$$0 = \sum_{i=1}^{3}\left[\left(\frac{\pi a^3}{12Z}\boldsymbol{N}_i\cdot\boldsymbol{D} - \omega\boldsymbol{S}\cdot\boldsymbol{R}_i\right)\boldsymbol{T}_i\cdot\boldsymbol{R}_i + \left(\zeta B_i\boldsymbol{T}_i\cdot\boldsymbol{D} - \omega\boldsymbol{S}\cdot\boldsymbol{R}_i\right)\boldsymbol{N}_i\cdot\boldsymbol{R}_i\right]$$

This is linear in ω and is rearranged to give

$$\omega = \frac{\sum_{i=1}^{3}\left[\frac{\pi a^3}{12Z}\boldsymbol{N}_i\cdot\boldsymbol{D}\cdot\boldsymbol{R}_i\,\boldsymbol{T}_i\cdot\boldsymbol{R}_i + \zeta B_i\,\boldsymbol{T}_i\cdot\boldsymbol{D}\cdot\boldsymbol{R}_i\,\boldsymbol{N}_i\cdot\boldsymbol{R}_i\right]}{\sum_{i=1}^{3}\left[\frac{\pi a^3}{12Z}\boldsymbol{N}_i\cdot\boldsymbol{S}\cdot\boldsymbol{R}_i\,\boldsymbol{T}_i\cdot\boldsymbol{R}_i + \zeta B_i\,\boldsymbol{T}_i\cdot\boldsymbol{S}\cdot\boldsymbol{R}_i\,\boldsymbol{N}_i\cdot\boldsymbol{R}_i\right]} \qquad (23)$$

Note that this expression is cyclic in the indices 1..3 as required from the definitions of $\mathbf{B}_i$ (Fig. 1).

6.2. Viscosity tensor

The angular velocity (23) is substituted back into Eq. (22) to give the forces on each boundary, which in turn substitute in Eq. (13) to give the stress as a function of deformation rate. The stress is adjusted to be trace-free since the hydrostatic

component has no effect on the creep rate. The actual analysis is implemented via symbolic mathematics in Maple via Matlab (code available from the author). It is easy to show that the antisymmetric part of **D** plays no role in the stress, as follows: express the antisymmetric part of **D** as α**S**. Since ω is linear in **D**, the antisymmetric part contributes α to ω and therefore contributes α**S** - α**S** = 0 to **D** - ω**S** , which is the only form in which **D** appears in the equations for force and stress.

Since **D** is volume-conserving, the relationship between stress and strain can be reduced to a linear dependence of a trace-free stress tensor on a symmetric trace-free strain rate tensor. This is of the form

$$@\sigma_{\alpha\beta} = \eta_{\alpha\beta\gamma\delta}\, \hat{e}_{\gamma\delta} \qquad (24)$$

making it clear that the dependence is via a fourth-rank viscosity tensor [9], which can also be expressed as its inverse, analogous to an elastic compliance tensor [10]. Compressive stress is taken as positive here. The tensor η is argued to have the same symmetries as the elastic stiffness [21],

$$\eta_{\alpha\beta\gamma\delta} = \eta_{\beta\alpha\gamma\delta}\,, \eta_{\alpha\beta\gamma\delta} = \eta_{\alpha\beta\delta\gamma}\,, \eta_{\alpha\beta\gamma\delta} = \eta_{\gamma\delta\alpha\beta} \qquad (25)$$

In 2D a symmetric tensor with zero trace only has two independent components, for example

$$\sigma = \begin{matrix} \sigma_{xx} & \sigma_{xy} \\ \sigma_{xy} & @\sigma_{xx} \end{matrix}$$

and can be represented by a 2D vector (Appendix 1). It is convenient to define a 2 x 2 viscosity matrix **H** so that

$$- \begin{matrix} \sigma_{xx} \\ \sigma_{xy} \end{matrix} = \begin{matrix} H_{11} & H_{12} \\ H_{21} & H_{22} \end{matrix} \begin{matrix} \hat{e}_{xx} \\ \hat{e}_{xy} \end{matrix} \qquad (26)$$

The third Eq. (25) ensures that **H** is symmetric, and its 3 components contain all the information about anisotropy. **H** does not transform like an ordinary tensor under rotations. However, note that if a symmetric matrix with zero trace is rotated by angle θ, its associated vector (Eq. (A1.1)) rotates by 2θ; hence the matrix **H** transforms under rotations like a rank 2 tensor except with double the angle. **H** has 2 eigenvectors, which indicate orientations in which the stress and strain rate tensors are parallel to each other. These eigenvectors are at 90° in this “double-angle” space. Therefore in real space there exist 4 orientations, spaced at 45° to each other, in which

the stress and strain rate tensors are parallel to each other. Two different eigenvalues indicate anisotropy. A polar plot of viscosity versus strain axis illustrates these properties (e.g. Fig. 4b).

My aim is to illustrate the effect of different grain shapes on rheology and grain rotation. I use 4 sets of hexagonal shapes governed by a single parameter λ, such that λ = 0 represents a regular hexagon in each set (Figure 2 and Table 2). Quantities are non-dimensionalised for simplicity, as follows: let a be a characteristic grain size parameter, and $\dot{\bar{\varepsilon}}^A$ a strain rate. Then:

$$\begin{aligned} \boldsymbol{B}^C &= \frac{\boldsymbol{B}}{a} \\ \boldsymbol{D}^C &= \frac{\boldsymbol{D}}{\dot{\bar{\varepsilon}}^A} \\ \sigma^C &= \sigma \frac{}{a^3} \\ \boldsymbol{H}^C &= \frac{\boldsymbol{H}}{a^3} \\ \omega^C &= \frac{\omega}{\dot{\bar{\varepsilon}}^A} \\ \zeta^C &= 36\zeta \frac{}{a^2} \end{aligned} \qquad (27)$$

7. Behaviour when boundaries do not support shear stress

This is the usual situation to be considered [2, 5, 22]; the terms in ζ are set to zero.

7.1 Kinematics

Figure 3 illustrates the response of the four types of shape in Figure 2 to pure shear (with extension parallel to y-axis) and simple shear (top-to-right, parallel to x axis). In the latter deformation, the principal axis of extension is 45° clockwise of the x axis. Fig. 3(b) shows that for pure shear, more elongate grains (larger λ) may show slower rotations but not necessarily (e.g. Hex4). Fig. 3(c, d) shows different rotation behaviours for simple shear. It is notable that some grains rotate the same way as the imposed shear, others counter to it. For shapes near that of a hexagon, very large angular velocities are predicted, with magnitudes far in excess of any invariant expressing magnitude of the strain rate. For example Hex1 in simple shear has grains rotating clockwise at 2.23 for an imposed deformation rate of 1.

Figure 3(a, c) also shows the instantaneous precipitation rates on each of the three faces. In pure shear, grains in Hex1 show precipitation on the top and symmetric dissolution on the two side faces as expected. In simple shear (Fig. 3((c) and (d)), however, all precipitation rates are zero, because sliding and grain rotation together are sufficient to take up the deformation, for that instant. This would also be the case if the deformation were a pure shear imposed at 45° to the axes, because the rotational component of deformation does not affect the precipitation rates. This "sliding only" response is the case for any value of λ in Hex1 and in Hex4. It has major implications for the strength of the polycrystal, discussed in section 6.2.

Before that, though, the limit $\lambda \rightarrow 0$ demands discussion.

7.1.1 Singular solutions and associated grain shapes

For all types of shape in Fig. 3 the limit $\lambda \rightarrow 0$ is a regular hexagon. One would expect, then, that for a particular imposed deformation a unique angular velocity will be predicted as $\lambda \rightarrow 0$ for all 4 types of hexagon. In fact, in pure shear there may be a limiting value for ω as $\lambda \rightarrow 0$ (Hex1, Hex4), or not (Hex2, Hex3). The same is true for simple shear (Fig. 3(d)) so it appears there is no unique solution for the angular velocity of a regular hexagon during diffusion creep. This may seem surprising but is easily explained. The numerator and denominator in Eq. (23) both contain terms $\boldsymbol{T}_i \cdot \boldsymbol{R}_i$. Each term is the dot product of a grain boundary vector with the translation vector which relates it to its symmetric equivalent. But in a regular hexagon, each boundary is perpendicular to its translation vector (Fig. 1) – so all these dot products disappear, and Eq. (23) takes the indeterminate form 0/0. This result has not been noted by other authors who used specific deformations and *assumed* zero angular velocity. Physically, it is because in each pair of boundaries, the two are directly opposite each other. Thus, not only forces but also moments cancel automatically.

This singular behaviour is not restricted to regular hexagons. Consider a hexagon with two sides defined by arbitrary vectors $\mathbf{B}_1$ and $\mathbf{B}_2$. Now define the third side by

$$\boldsymbol{B}_3 = \frac{\boldsymbol{B}_1 \cdot \boldsymbol{B}_2}{\boldsymbol{B}_1 \times \boldsymbol{B}_2} \boldsymbol{S}^{b} \boldsymbol{B}_1 \otimes \boldsymbol{B}_2^{c} \qquad (28)$$

It is trivial to show that $\boldsymbol{T}_i \cdot \boldsymbol{R}_i = 0$ for all sides. Consequently, recalling $\zeta = 0$, the denominator in Eq. (23) is zero. An arbitrary irregular hexagon is defined here by 6

independent parameters; ignoring size and orientation this means the basic shape is defined by 4 parameters. Eq. (28) shows that a subset, defined by 2 parameters, of all hexagonal shapes will yield singular behaviour in the model discussed here. An example is shown in Fig. 2.

The existence of this singular subset is significant. Small perturbations of shape from any shape in that subset will give rise to a great range of angular velocities, because the denominator in Eq. (23) will be small. One thus expects a great variety of rotation behaviours for quite subtly different grain shapes. Microstructures which bear some similarity to "ordinary" hexagonal shapes will not show such extreme angular velocities.

Regular hexagons are the simplest idealisation of equi-axed grains, but they belong to the singular subset. This is the underlying explanation for why irregular networks of (on average) equi-axed grains give rise to such a wide range of angular velocities (Fig. 1 in [8]).

7.2 Dynamics

The viscosity tensor can be obtained by calculating the stress for 2 different strain rate tensors using Eqs. (13), (22) and (23), normalising the trace of the stress to zero in each case, and then using Eq. (26). The result is a function of the 6 variables that define $\mathbf{B}_{1..3}$, and is too long to write out in full. Symbolic routines in Maple via Matlab, however, allow analysis of the situation, in particular an examination of the viscosity anisotropy. Before describing some specific examples, I discuss the result that for a completely general set of boundaries, when they cannot support shear stress,

$$\det \mathbf{H} = 0 \qquad (29)$$

so that $\mathbf{H}$ has one eigenvalue equal to zero. This is a remarkable result, because it implies that any microstructure formed by periodic irregular hexagons has one direction in double-angle space which has zero viscosity. In actual space 2 directions at right angles will have zero viscosity. The result implies that there exists a particular strain rate tensor for which the stress is zero, and consequently the force on each boundary is zero, so that from Eq. (20), all precipitation rates are zero. The deformation in this case is accomplished purely by sliding and grain rotation: two examples have already been shown of imposed deformations giving rise to this response (simple shear of Hex1 and Hex4, Fig. 3). Since in this section we are considering inviscid grain boundaries, no stress is required to accomplish deformation

by sliding. Equation (29) implies that there are 2 "zero-strength" directions for any polycrystal made of irregular hexagons. We can determine the “zero strength” directions from the eigenvectors of **H**. It is more illuminating, though, to use the kinematic equations (6) to determine the “zero strength” direction, by solving the three equations $u_{1..3} = 0$ for **D**. If two of these equations are satisfied, the third will be automatically, because of mass conservation (Eq. (19)). Writing out the equations for the first two boundaries, we have:

$$\boldsymbol{N}_1 \cdot \boldsymbol{D} \otimes \omega \boldsymbol{S} \cdot \boldsymbol{R}_1 = 0$$
$$\boldsymbol{N}_2 \cdot \boldsymbol{D} \otimes \omega \boldsymbol{S} \cdot \boldsymbol{R}_2 = 0$$

D has 3 unknown components, so we can set ω to zero to obtain 2 equations in 3 unknowns. Solving gives a value for **D** (except for an arbitrary constant of multiplication) as a function of the grain shape as defined by $\mathbf{B}_{1..3}$. Appendix 2 shows that the solution is:

$$\boldsymbol{D}_w = \boldsymbol{G}\boldsymbol{S} \qquad (30)$$

where **G** is a symmetric tensor given by:

$$\boldsymbol{G} = \boldsymbol{B}_2 \otimes \boldsymbol{B}_3 - \boldsymbol{B}_1 \cdot \boldsymbol{B}_1 + \boldsymbol{B}_3 \otimes \boldsymbol{B}_1 - \boldsymbol{B}_2 \cdot \boldsymbol{B}_2 + \boldsymbol{B}_1 \otimes \boldsymbol{B}_2 - \boldsymbol{B}_3 \cdot \boldsymbol{B}_3 \qquad (31)$$

Note that **G** is cyclic in the indices 1 to 3 as expected from the initial definitions of the vectors (Fig. 1). The weak directions can be determined from the symmetric part of $\mathbf{D}_w$, namely

$$\boldsymbol{E}_w = \frac{\boldsymbol{D}_w + \boldsymbol{D}_w^T}{2} \qquad (32)$$

The eigenvectors of $\mathbf{E}_w$ give the two weak directions.

7.3 Example Hex1

This is a symmetric hexagon, elongate parallel to the x-axis. We find:

$$\boldsymbol{H}^c = \begin{bmatrix} \frac{1}{72}\left(1 + \frac{3\lambda^{c_2}}{0}\right) & 0 \\ 0 & 0 \end{bmatrix} \qquad (33)$$

The eigenvector corresponding to the weak directions is (0, 1) in double-angle space, corresponding to two axes at 45° to the x-axis in real space, regardless of the value of λ. This can be understood by noting that the weak axes must be at 90° to each other, but must also satisfy the symmetry of the grain. This has vertical and horizontal

mirror planes, so only 0°, 45° and 90° are allowed. 0° and 90° are strong directions. The limit as $\lambda \to 0$ is

$$\boldsymbol{H}^{c} = \frac{1}{72}\begin{bmatrix} 1 & 0 \\ 0 & 0 \end{bmatrix} \tag{34}$$

which will be compared with the limit for a different parameterisation now.

7.4 Example Hex2

This is a distorted hexagonal shape with no mirror symmetry. Here we have:

$$\boldsymbol{H}^{c} = \frac{1}{216}\begin{bmatrix} \lambda^{2} & -\sqrt{3}\lambda \\ -\sqrt{3}\lambda & 3 \end{bmatrix} \tag{35}$$

The non-zero eigenvalue is

$$H_{s}^{c} = \frac{1}{216}\lambda^{2} + \frac{1}{72} \tag{36}$$

and the eigenvector of **H** corresponding to the weak direction is, in double-angle space,

$$\frac{1}{\sqrt{3+\lambda^{2}}}\left(\sqrt{3}, \lambda\right)$$

which in actual space corresponds to two orthogonal directions

$$\left(\frac{3+\lambda^{2}+\sqrt{3}}{\lambda}, 1\right). \tag{37}$$

Note that for large λ these approach 45° to the coordinate axes, but this example shows that in general the weak directions relate in a complicated fashion to the grain shape, unless that grain has mirror symmetry (Hex1).

The viscosity limit as $\lambda \to 0$ is

$$\boldsymbol{H}^{c} = \frac{1}{72}\begin{bmatrix} 0 & 0 \\ 0 & 1 \end{bmatrix} \tag{38}$$

with weak directions parallel to x and y axes. This value differs in orientation from that derived for Hex1 (Eq. (34)), illustrating that no unique value of viscosity exists for the rheology of an array of regular hexagons (or for other “singular” shapes).

The parameterisation using λ does not necessarily represent the subsequent evolution of this shape; it is intended just to illustrate the responses of grains which have shapes as a function of one parameter.

8. Behaviour when boundaries support shear stress

If ζ is non-zero, the denominator in Eq. (23) is non-zero for any shape, and now the viscosity for regular hexagons is well-defined and isotropic:

$$\boldsymbol{H}^{c} = \frac{1}{72}\begin{pmatrix} 10 & 0 \\ 0 & 1 \end{pmatrix} \tag{39}$$

This is the simplest illustration that grain boundary viscosity increases the overall viscosity of the polycrystals,

To examine the general way in which ζ affects rheology, consider the derivation of the stress tensor for a particular deformation rate. From Eq. (23) the numerator and denominator of ω are linear in ζ

$$\omega = \frac{J_0 + J_1 \zeta}{A_0 + A_1 \zeta} \tag{40}$$

where the Js are a function of geometry and deformation rate, and the As a function of geometry. From Eqs. (22) and (13), we see that

$$\sigma = A^{a} + A^{a}\zeta + \zeta\left(A^{a} + A^{a}\omega\right)$$

Where (A) is shorthand for an (unspecified) function of geometry and deformation rate; this is sufficient to show that **σ** is of the form (quadratic in ζ)/(linear in ζ), and hence the viscosity is:

$$\boldsymbol{H} = \frac{\boldsymbol{H}_0 + \boldsymbol{H}_1\zeta + \boldsymbol{H}_2\zeta^2}{1 + A_1\zeta} \tag{41}$$

Here $\mathbf{H}_0$ is the viscosity in the absence of grain boundary viscosity. For large ζ, **H** is linear in ζ. The viscosity of a polycrystal made of irregular hexagons is in general still strongly anisotropic.

8.1 Example Hex1

The elongate hexagon has mirror symmetry so, as in the case for zero ζ, the two weak directions are at 45° to the coordinate axes in actual space; in double angle space the eigenvectors of **H** are parallel to the coordinate axes and the off-diagonal terms are zero.

$$H_{11}^C = \frac{1}{72}\left(1+\sqrt{3}\,\lambda\right)^{c_2} + \frac{1}{72}\left(1+\frac{\lambda^2}{3+2\sqrt{3}\,\lambda}\right)\zeta^C$$

$$H_{22}^C = \frac{1}{36}\,\frac{\left(\sqrt{3}+2\lambda\right)^{cd}\left(\sqrt{3}+\lambda+\sqrt{3}+3\lambda\right)^{ce}\zeta^{c}\zeta^{c}\sqrt{3}}{\sqrt{3}\,\lambda^2+6\sqrt{3}+18\lambda+3\sqrt{3}\,\lambda^2}\zeta^C \qquad (42)$$

$$H_{12}^C = H_{21}^C = 0$$

H_{22} exhibits the general form of viscosity dependence on ζ^* while, for H_{11}, the denominator is a factor of the numerator, leaving a linear dependence on ζ. For $\zeta = 0$, H_{11} has the limit as in Eq. (33) and H_{22} becomes zero. Fig 4(a) illustrates the dependence of the eigenvalues on ζ^* for $\lambda = 2$. There is a particular value at which the viscosity is isotropic, but as ζ increases, anisotropy remains.

8.2 Example Hex2

The viscosity tensor as a function of ζ^* and λ is too long to write out, so for illustration substitute $\lambda = (1/4)\sqrt{3}$, the value being chosen because then the length of side 3 (vector $\mathbf{B}_3$) is 5/4 that of the other two sides which leads to relatively simple exact expressions for the viscosity tensor.

$$H_{11}^C = \frac{1}{3456}\,\frac{945+63013\zeta^C+63294\,\zeta^{c_2}}{315+926\zeta^C}$$

$$H_{12}^C = @\frac{1}{288}\,\frac{315@1489\zeta^C+1434\,\zeta^{c_2}}{315+926\zeta^C} \qquad (43)$$

$$H_{22}^C = \frac{1}{72}\,\frac{315+1871\zeta^C+858\,\zeta^{c_2}}{315+926\zeta^C}$$

Substituting $\zeta^* = 0$ gives a viscosity consistent with Eq. (35) with the appropriate value of λ. Fig. 4(b) shows how both eigenvalues increase with ζ^*. Because this grain shape is not orthorhombic, the eigenvectors are not constrained by symmetry and rotate with ζ^* (Fig. 4(c)).

9. Discussion

9.1 Time evolution

My aim here is to give a complete analytic treatment of the instantaneous response of a periodic microstructure in diffusion creep. Building on this, the evolution through time can be modelled, as two examples show (Fig. 5). These were produced using a numerical modelling program developed previously for diffusion creep [2], extended to incorporate periodic microstructures and boundary conditions [8]. Analytic solutions cannot be obtained for this because of the way that new grain boundary and triple junction positions are calculated [2]. There is no inconsistency between the numerical and analytic modelling. The analytic treatment here was motivated by the need to understand the results of the numerical simulations, which are frequently counter-intuitive.

9.2 Grain rotation

Grain rotation is an integral part of the deformation. For nearly hexagonal shapes, large angular velocities are predicted, especially when no shear stress is assumed along grain boundaries. This is because the regular hexagon shape actually yields a singular solution. I suggest that complicated microstructures can be considered – to a degree – as perturbed versions of periodic hexagonal microstructures. The unbounded angular velocities predicted here for nearly regular hexagons then provide an explanation for the wide range of angular velocities predicted in numerical models of irregular grain networks when those grains are on average equi-axed [8]. Equally importantly, if grains do for any reason become elongate, the angular velocities are much reduced in many cases (e.g. Fig. 3).

9.3 Anisotropic viscosity

It has been shown that a periodic microstructure made from a single irregular hexagonal grain shape has marked viscosity anisotropy during diffusion creep. The anisotropy is manifest in two orthogonal strong directions, and two orthogonal weak directions at 45° to the strong directions. In the absence of grain boundary viscosity, the weak directions have zero strength. Coaxial stretching parallel to a weak direction thus requires, for an instant, no stress. Simple shear with a shear plane at 45° to a weak direction (i.e. shear plane parallel to a strong direction) also requires no stress.

This behaviour arises because grain boundary sliding is always one aspect of diffusion creep, and there is always an orientation of strain in which sliding alone is a sufficient response, without dissolution and precipitation of material at grain boundaries. If finite shear strength is assigned to grain boundaries, anisotropy remains but now the polycrystal has non-zero viscosity in all directions. Both viscosity eigenvalues increase as the grain boundary viscosity ζ increases if other quantities are fixed.

When grains are elongate the periodic microstructure discussed here is anisotropic, with or without grain boundary shear stresses. It is to be expected then that irregular aggregates of shaped grains will be anisotropic, and this will have implications for the way in which strain partitions and perhaps localises during diffusion creep and superplasticity.

9.4 Relationship to previous work

Lifshitz [9] pointed out that diffusion creep is likely to give rise to anisotropic viscosity, with the emphasis on volume diffusion creep but a preliminary treatment of grain boundary diffusion creep in his Appendix 3. He made no explicit mention of grain rotation and so it remains unclear how this would affect the predictions. Greenwood [23] provided a precise expression for the anisotropic response of an orthorhombic grain during Nabarro-Herring creep, but under special stress orientations. Greenwood [10] provided expressions for the viscosity tensor under more general stress orientations. In that work it was assumed that creep strength varies smoothly as the stress axes are rotated, so that there are no maxima or minima at intermediate positions. This contribution, however, shows that there may be marked strength minima at 45 degrees to strength maxima, so it would be interesting to see how the different approaches could be reconciled. Again, the effects of grain rotation must be considered.

Separate strands of research have examined certain restricted types of hexagonal arrays under restricted deformation conditions. For hexagons with mirror symmetry in pure shear [12], the analysis here is in agreement. Specifically, the stretched hexagonal shapes are of the form Hex1, with the parameter λ related to the finite strain. In pure shear, the H_{11} component (from Eq. (42)) defines the stress and it can be shown that this is equivalent to equations 11, 13 and 14 of Kim et al. [12]. However the latter analysis did not encompass different strain directions, and hence does not address anisotropy.

Raj and Ashby[5] show a regular hexagonal array and draw zigzag surfaces of connected grain boundary segments which they identify as Mode 1 and Mode 2 sliding surfaces (their Fig. 2.3). They then analyse movement accommodated by diffusion along such serrated surfaces. There appears to be a distinction made between the slip surfaces and apparently rigid polycrystals on each side. If, however, all grain boundaries are assigned the same properties, they must all be involved in sliding and accommodating strain and hence the picture presented by those authors becomes modified. Kim et al. [14] allow all grains to rotate and derive a flow stress for shear (their equation 19) which can be shown to agree with Eq. (39) given here when there is grain boundary viscosity. This work does not reveal the singular nature of the regular hexagonal array in the absence of grain boundary viscosity, however; nor does it reveal the large and disparate angular velocities and strengths to be expected under different loading conditions and for grain shapes slightly different from regular.

In summary, this contribution shows how the grain rotations and strength properties of a periodic array of irregular hexagons may be predicted in a unified fashion. Some previous work can be seen as particular examples of this more general theory. The new theory highlights the importance of strength anisotropy and of the effect of overall grain shapes on grain rotation during diffusion creep: it provides a platform for understanding the behaviour of more complicated microstructures.

References

[1] J. Pan and A.C.F. Cocks, Computational Materials Science **1** 95 (1993)
[2] J.M. Ford, J. Wheeler and A.B. Movchan, Acta Materialia **50** 3941 (2002)
[3] R. Ding, D. Moldovan, V. Yamakov, et al., Modelling And Simulation In Materials Science And Engineering **13** 1129 (2005)
[4] M.R. Drury and J.D. Fitz Gerald, in: *Earth's Mantle: Composition, Structure and Evolution*, I. Jackson, ed. (Cambridge University Press, Cambridge, 1998)
[5] R. Raj and M.F. Ashby, Metallurgical Transactions **2** 1113 (1971)
[6] T. Mori, S. Onaka and K. Wakashima, Journal of Applied Physics **83** 7547 (1998)
[7] W. Beere, Philosophical Transactions of the Royal Society of London A **288** 177 (1978)
[8] J. Wheeler, Geophysical Journal International **178** 1723 (2009)
[9] I.M. Lifshitz, Soviet Physics JETP **17** 909 (1963)
[10] G.W. Greenwood, Proceedings of the Royal Society of London Series a-Mathematical Physical and Engineering Sciences **436** 187 (1992)

[11] P.M. Hazzledine and J.H. Schneibel, Acta Metallurgica et Materialia **41** 1253 (1993)
[12] B.N. Kim, K. Hiraga, K. Morita, et al., Philosophical Magazine **84** 3251 (2004)
[13] W. Beere, Journal Of Materials Science **12** 2093 (1977)
[14] B.N. Kim, K. Hiraga, K. Morita, et al., Acta Materialia **57** 5730 (2009)
[15] R. Hill, Journal Of The Mechanics And Physics Of Solids **11** 357 (1963)
[16] T. Mura, *Micromechanics of defects in solids* (Kluwer Academic Publishers, Dordrecht ; London 1987)
[17] G.J. Rodin, Journal of Applied Mechanics-Transactions of the ASME **62** 1 (1995)
[18] A.C.F. Cocks, S.P.A. Gill and J.Z. Pan, in: *Advances in Applied Mechanics* 36 (Academic Press, 1999)
[19] B.N. Kim, K. Hiraga and K. Morita, Acta Materialia **53** 1791 (2005)
[20] T.S. Ke, Metallurgical And Materials Transactions A-Physical Metallurgy And Materials Science **30** 2267 (1999)
[21] R.C. Wajsowicz, Journal Of Computational Physics **105** 333 (1993)
[22] J.R. Spingarn and W.D. Nix, Acta Metallurgica **26** 1389 (1978)
[23] G.W. Greenwood, Philosophical Magazine a-Physics of Condensed Matter Structure Defects and Mechanical Properties **51** 537 (1985)

Appendix 1: transformation properties of H

It is shown here that the viscosity tensor in actual space can be related to **H** which transforms like a tensor under rotations in a "double angle" space. Let **P** be any symmetric tensor with zero trace, so it has just 2 independent parts, P_{xx} and P_{xy}.

$$\underset{c}{\boldsymbol{P}} = \begin{pmatrix} P_{xx} & P_{xy} \\ P_{xy} & -P_{xx} \end{pmatrix}$$

The effect of an anticlockwise rotation through θ

$$\underset{c}{\boldsymbol{O}}(\theta) = \begin{pmatrix} \cos\theta & -\sin\theta \\ \sin\theta & \cos\theta \end{pmatrix}$$

on **P** is

$$\underset{c}{\boldsymbol{P}}' = \underset{c}{\boldsymbol{O}}(\theta)\,\underset{c}{\boldsymbol{P}}\,\underset{c}{\boldsymbol{O}}(-\theta) = \begin{pmatrix} P_{xx}\cos 2\theta - P_{xy}\sin 2\theta, & P_{xy}\cos 2\theta + P_{xx}\sin 2\theta \\ P_{xy}\cos 2\theta + P_{xx}\sin 2\theta, & P_{xy}\sin 2\theta - P_{xx}\cos 2\theta \end{pmatrix}$$

Representing **P** by a 2-element vector

$$\underset{c}{\boldsymbol{p}} = \begin{pmatrix} P_{xx} \\ P_{xy} \end{pmatrix} \qquad \text{(A1.1)}$$

it is seen that

$$\boldsymbol{p}_c = \begin{bmatrix} P_{xx}\cos 2\theta + P_{xy}\sin 2\theta \\ P_{xy}\cos 2\theta + P_{xx}\sin 2\theta \end{bmatrix} = \begin{bmatrix} \cos 2\theta & \sin 2\theta \\ \sin 2\theta & \cos 2\theta \end{bmatrix} \boldsymbol{p}_c = \boldsymbol{O}_c(2\theta)\boldsymbol{p}_c \qquad \text{(A1.2)}$$

Thus, all tensors **P** can be represented as 2-vectors of the form **p**, which transform as if rotated by 2θ when the tensor **P** is rotated by θ. A linear relationship between two such tensors in actual space is represented by a 4th rank tensor. In double angle space the linear relationship can be expressed by a second rank tensor which as a consequence of (A1.2) transforms like an ordinary tensor under rotations but with double the angle:

$$\boldsymbol{H}_c = \boldsymbol{O}_c(2\theta)\boldsymbol{H}_c\boldsymbol{O}_c(2\theta) \qquad \text{(A1.3)}$$

Appendix 2: equations for zero strength directions

Rather than give the derivation, it is sufficient to show that $\mathbf{D}_w$ as defined using **G** in Eq. (30) satisfies

$$\boldsymbol{N}_i \cdot \boldsymbol{D}_w \boldsymbol{R}_i = 0 \qquad \text{(A2.1)}$$

using any value of i. Consider the vector

$$\begin{aligned}
&\boldsymbol{D}_w \boldsymbol{R}_1 = \boldsymbol{G}\boldsymbol{S}\left[\boldsymbol{B}_2 \otimes \boldsymbol{B}_3\right] = \\
&\left[\boldsymbol{B}_2 \otimes \boldsymbol{B}_3\right]\boldsymbol{B}_1\left[\boldsymbol{B}_1 + \boldsymbol{B}_3 \otimes \boldsymbol{B}_1\right]\boldsymbol{B}_2\left[\boldsymbol{B}_2 + \boldsymbol{B}_1 \otimes \boldsymbol{B}_2\right]\boldsymbol{B}_3\left[\boldsymbol{B}_3\right]\boldsymbol{S}\left[\boldsymbol{B}_2 \otimes \boldsymbol{B}_3\right] = \\
&\left[\boldsymbol{B}_2 \otimes \boldsymbol{B}_3\right]\boldsymbol{B}_1\left[\boldsymbol{B}_1\right]\cdot\boldsymbol{S}\left[\boldsymbol{B}_2\right] + \left[\boldsymbol{B}_3 \otimes \boldsymbol{B}_1\right]\boldsymbol{B}_2\left[\boldsymbol{B}_2\right]\cdot\boldsymbol{S}\left[\boldsymbol{B}_2\right] + \left[\boldsymbol{B}_1 \otimes \boldsymbol{B}_2\right]\boldsymbol{B}_3\left[\boldsymbol{B}_3\right]\cdot\boldsymbol{S}\left[\boldsymbol{B}_2\right] \otimes \\
&\left[\boldsymbol{B}_2 \otimes \boldsymbol{B}_3\right]\boldsymbol{B}_1\left[\boldsymbol{B}_1\right]\cdot\boldsymbol{S}\left[\boldsymbol{B}_3\right] \otimes \left[\boldsymbol{B}_3 \otimes \boldsymbol{B}_1\right]\boldsymbol{B}_2\left[\boldsymbol{B}_2\right]\cdot\boldsymbol{S}\left[\boldsymbol{B}_3\right] + \left[\boldsymbol{B}_1 \otimes \boldsymbol{B}_2\right]\boldsymbol{B}_3\left[\boldsymbol{B}_3\right]\cdot\boldsymbol{S}\left[\boldsymbol{B}_3\right] = \\
&\left[\boldsymbol{B}_2 \otimes \boldsymbol{B}_3\right]\boldsymbol{B}_1\left[\boldsymbol{B}_1\right]\cdot\boldsymbol{S}\left[\boldsymbol{B}_2\right] + \left[\boldsymbol{B}_1 \otimes \boldsymbol{B}_2\right]\boldsymbol{B}_3\left[\boldsymbol{B}_3\right]\cdot\boldsymbol{S}\left[\boldsymbol{B}_2\right] \otimes \\
&\left[\boldsymbol{B}_2 \otimes \boldsymbol{B}_3\right]\boldsymbol{B}_1\left[\boldsymbol{B}_1\right]\cdot\boldsymbol{S}\left[\boldsymbol{B}_3\right] \otimes \left[\boldsymbol{B}_3 \otimes \boldsymbol{B}_1\right]\boldsymbol{B}_2\left[\boldsymbol{B}_2\right]\cdot\boldsymbol{S}\left[\boldsymbol{B}_3\right] = \\
&\left[\boldsymbol{B}_2 \otimes \boldsymbol{B}_3\right]\left[\boldsymbol{B}_2 \otimes \boldsymbol{B}_1\right] \otimes \left[\boldsymbol{B}_2 \otimes \boldsymbol{B}_3\right]\boldsymbol{B}_1\left[\boldsymbol{B}_3 \otimes \boldsymbol{B}_1\right]\boldsymbol{B}_1 + \\
&+ \left[\boldsymbol{B}_1 \otimes \boldsymbol{B}_2\right]\boldsymbol{B}_3\left[\boldsymbol{B}_2 \otimes \boldsymbol{B}_3\right] \otimes \left[\boldsymbol{B}_3 \otimes \boldsymbol{B}_1\right]\boldsymbol{B}_2\left[\boldsymbol{B}_3 \otimes \boldsymbol{B}_2\right] =
\end{aligned} \qquad \text{(A2.2)}$$

where terms of the form **a.Sa** are identically zero. Now consider the last two terms, and define

$$\boldsymbol{Q} = \left[\boldsymbol{B}_1 \otimes \boldsymbol{B}_2\right]\boldsymbol{B}_3\left[\boldsymbol{B}_2 \otimes \boldsymbol{B}_3\right] \otimes \left[\boldsymbol{B}_3 \otimes \boldsymbol{B}_1\right]\boldsymbol{B}_2\left[\boldsymbol{B}_3 \otimes \boldsymbol{B}_2\right] \qquad \text{(A2.3)}$$

Noting that

$$\boldsymbol{a} \times \boldsymbol{b} = -\boldsymbol{b} \times \boldsymbol{a}$$

we have

$$\boldsymbol{Q} \times \boldsymbol{B}_1 = \boldsymbol{B}_1 \times \boldsymbol{B}_2 \, \boldsymbol{B}_3 \times \boldsymbol{B}_1 \, \boldsymbol{B}_2 \times \boldsymbol{B}_3 - \boldsymbol{B}_3 \times \boldsymbol{B}_1 \, \boldsymbol{B}_2 \times \boldsymbol{B}_1 \, \boldsymbol{B}_3 \times \boldsymbol{B}_2 = 0$$

Hence **Q** is parallel to $\mathbf{B}_1$, so $\mathbf{D}_w\mathbf{R}_1$ is parallel to $\mathbf{B}_1$. Because $\mathbf{N}_1$ is orthogonal to $\mathbf{B}_1$ we have proved Eq. (A2.1) for i = 1. All expressions involved are cyclic with respect to indices 123, so it follows that Eq. (A2.1) holds for all i.

Tables

Table 1: Notation

Symbol	Meaning
B	Vector defining grain boundary
C	Current (flux x grain boundary width)
D	Deformation rate tensor
Dw	Deformation rate tensor giving rise to zero stress and zero grain rotation
f	Force per unit length as function of position
F	Force across boundary
H	2nd rank viscosity tensor (in "double angle" space)
L	Onsager diffusion coefficient
N	Unit vector perpendicular to (anticlockwise of) B = **ST**
R	Vector translating boundary to symmetrically equivalent position
s	Distance along a boundary segment
S	Skew tensor
t	Sliding velocity along boundary
T	Unit vector parallel to B
u	Divergence velocity of two grains (precipitation rate at their contact)
V	Molar volume
w	Effective grain boundary width
$\mathbf{w}_G$	Velocity of grain G measured at origin
Z	$=LV^2w$ (units of m^3/Pa/s)
$\boldsymbol{\eta}$	4th rank viscosity tensor
λ	Parameter defining a set of hexagon shapes, $\lambda = 0$ is regular
$\boldsymbol{\sigma}$	Stress
ω	Angular velocity
ζ	Ratio of shear stress to sliding velocity (units of Pas/m)

Table 2: The non-dimensionalised side vectors defining four families of hexagons, each parameterised by λ.

Regular hexagon	$\left\langle \frac{1}{2}, \frac{\sqrt{3}}{2} \right\rangle$	$\left\langle \frac{1}{2}, -\frac{\sqrt{3}}{2} \right\rangle$	$\langle 0, -\sqrt{3} \rangle$
*Hex*1	$\left\langle \frac{1}{2}, \frac{\sqrt{3}}{2} \right\rangle$	$\left\langle \frac{1}{2}, -\frac{\sqrt{3}}{2} \right\rangle$	$\langle 0, -\sqrt{3} \rangle + \lambda \left\langle \frac{1}{2}, \frac{\sqrt{3}}{2} \right\rangle$
*Hex*2	$\left\langle \frac{1}{2}, \frac{\sqrt{3}}{2} \right\rangle$	$\left\langle \frac{1}{2}, -\frac{\sqrt{3}}{2} \right\rangle$	$\langle 0, -\sqrt{3} \rangle + \lambda \left\langle \frac{1}{2}, -\frac{\sqrt{3}}{2} \right\rangle$
*Hex*3	$\left\langle \frac{1}{2}, \frac{\sqrt{3}}{2} \right\rangle$	$\left\langle \frac{1}{2}, -\frac{\sqrt{3}}{2} \right\rangle + \lambda \langle 1, 0 \rangle$	$\langle 0, -\sqrt{3} \rangle$
*Hex*2	$\left\langle \frac{1}{2}, \frac{\sqrt{3}}{2} \right\rangle + \lambda \langle 1, 0 \rangle$	$\left\langle \frac{1}{2}, -\frac{\sqrt{3}}{2} \right\rangle$	$\langle 0, -\sqrt{3} \rangle$

Captions to figures

Fig. 1. The meaning of the main geometric vectors defined here.

Fig. 2. Four different types of perturbed regular hexagonal shape, c.f. Table 1. Vertical height of regular hexagon is 1, so its sides are length $1/\sqrt{3}$. The last figure shows a "singular" hexagonal shape. Pairs of faces are directly opposite each other, so that moments as well as forces will always balance, giving rise to singular behaviour.

Fig. 3. Each row relates to one of the perturbed hexagonal shapes. Column **(a)**: the microstructure for a value of $\lambda = 0.5$, showing precipitation rates (numbers written beside each of 3 distinct sides) and angular velocity ω (rotation sense emphasised by curved arrow) for **D** = [-1/2 0; 0 1/2], stretching parallel to y axis. **(b)**: angular velocity as a function of λ for the same **D**. Cross marks value used in (a). **(c)**: the microstructure for a value of $\lambda = 0.5$, showing kinematic quantities as in (a) but for **D** = [0 1/2; 0 0], top-to-right simple shear parallel to x axis. **(d)**: angular velocity as a function of λ for the same **D**. Cross marks value used in (c).

Fig. 4. (a) Eigenvalues of the viscosity tensor as a function of ζ^* for a particular shape, Hex1 with $\lambda = 2$. The grain shape is shown bottom right. **(b)** Nested polar plots showing the viscosity as a function of the orientation of the maximum strain rate axis, for 4 values of ζ^*. **(c)** As (a), for Hex2 with $\lambda = (1/4)\sqrt{3}$. **(d)** Angle of "weak" direction to x-axis as a function of ζ^* for Hex2 as in (b). **(e)** Viscosity plots for Hex2; note that because Hex2 has no mirror plane, the orientation of the viscosity tensor can vary.

Fig. 5. Examples of evolution of a periodic microstructure through time in **(a)** simple shear and **(b)** pure shear. Numbers indicate times. The evolution of the xx and xy stresses is shown in **(c)** with solid lines corresponding to simple shear (a) and dashed lines for pure shear (b). The microstructure accommodates the first increment of strain at zero stress, but then as it evolves the principal strain rate directions are no longer aligned parallel to the "weak" directions and the stresses are non-zero. Note how in

(b) the grain shapes evolve in such a way as to strengthen and then weaken the microstructure as a neighbour-switching geometry is approached.

Wheeler Fig. 1

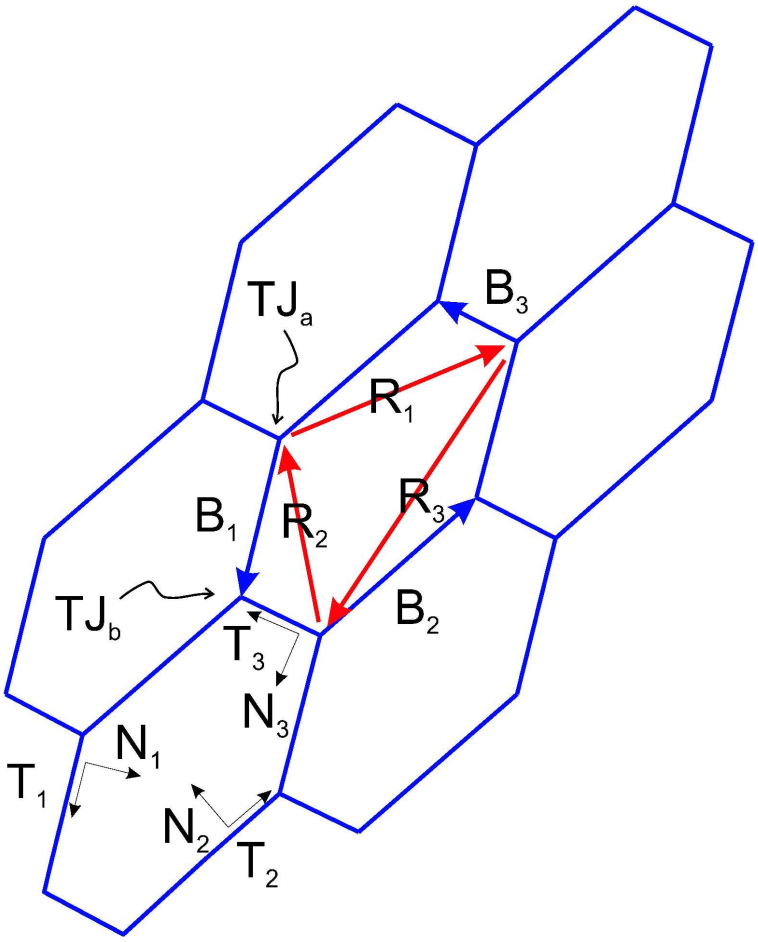

132x210mm (600 x 600 DPI)

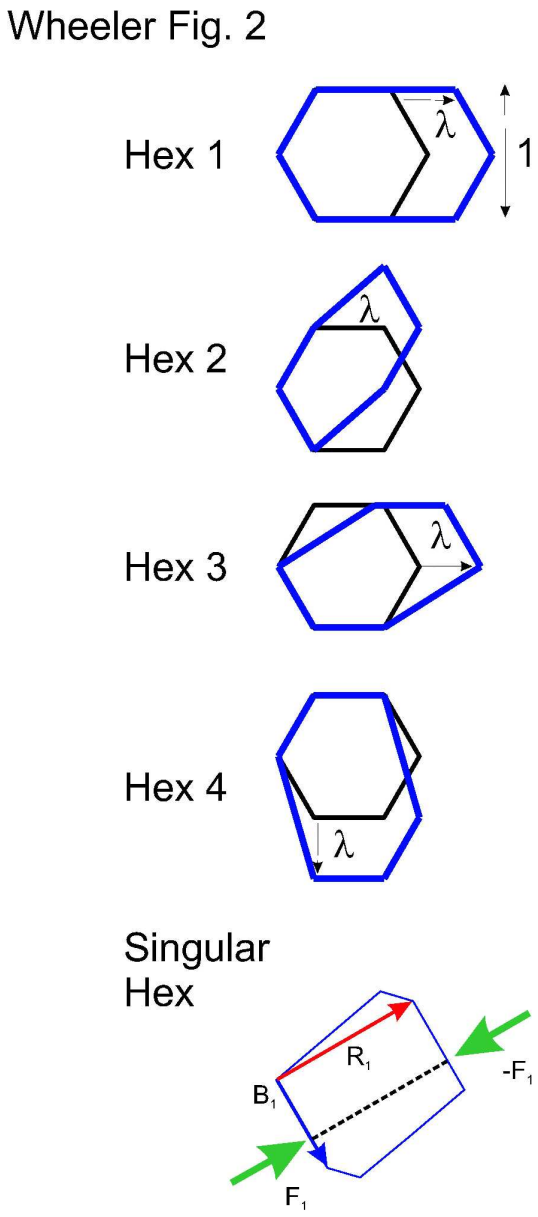

111x254mm (600 x 600 DPI)

Wheeler Fig. 3

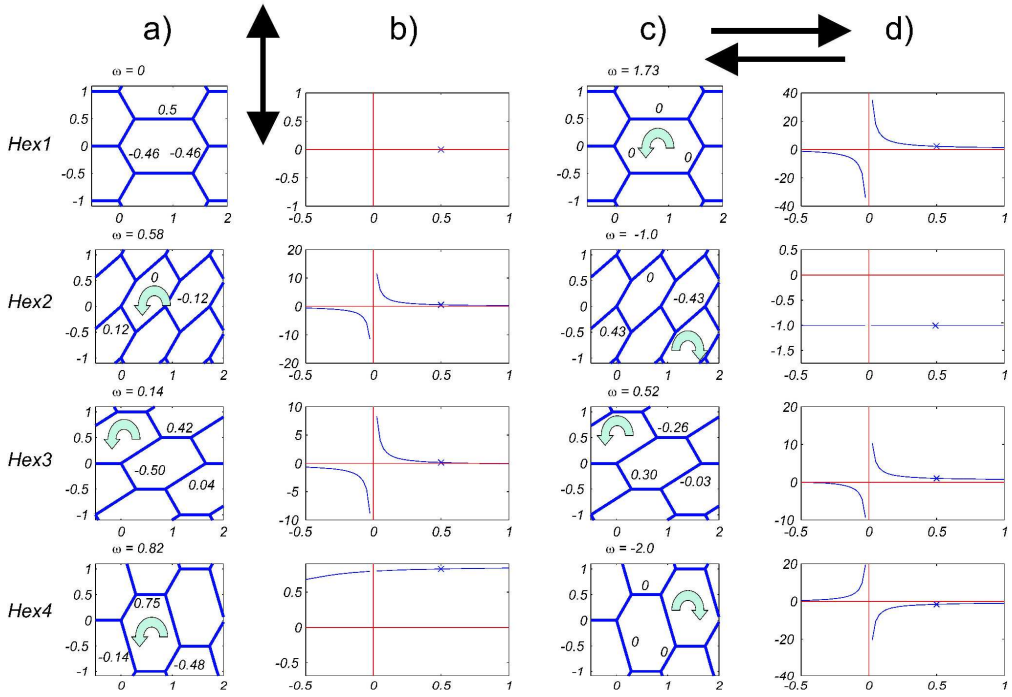

260x189mm (600 x 600 DPI)

Wheeler Fig.4

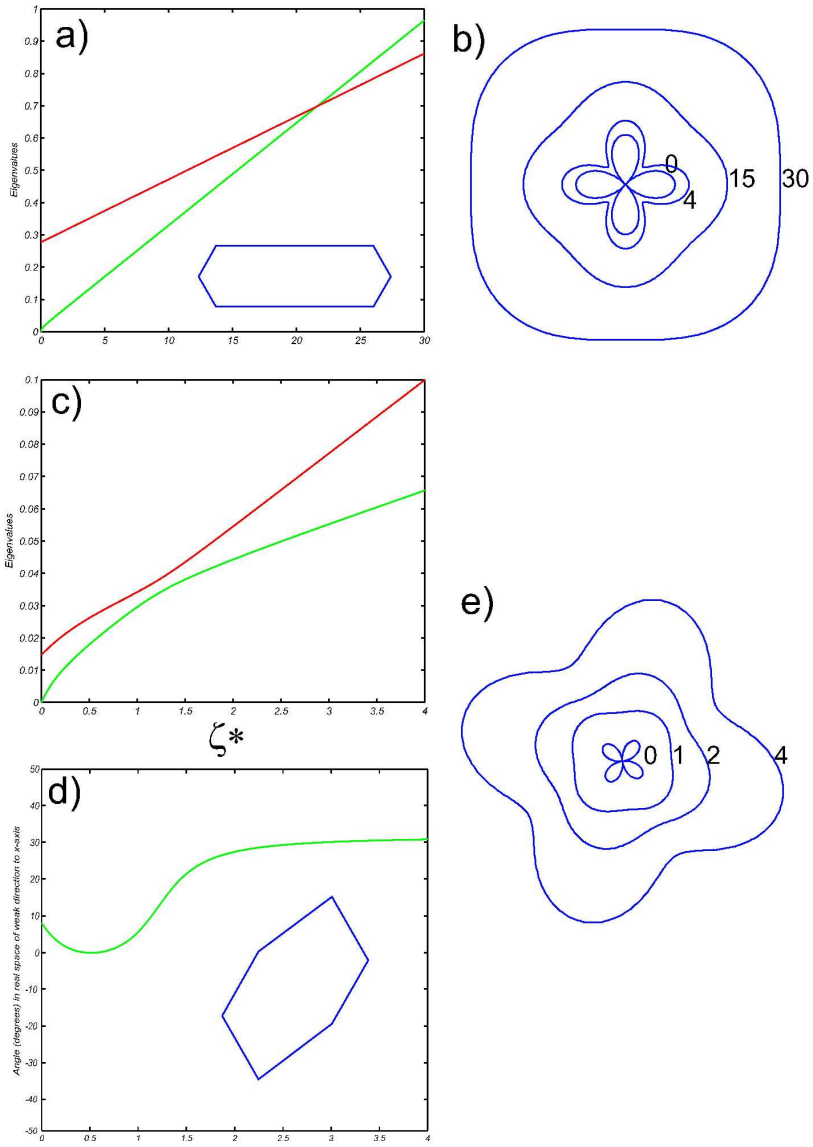

179x267mm (600 x 600 DPI)

Wheeler
Fig. 5

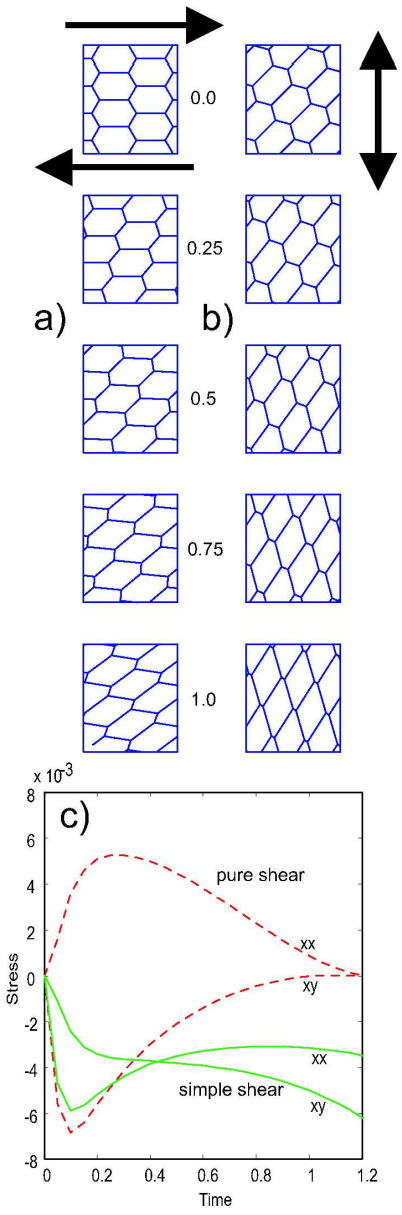

137x275mm (600 x 600 DPI)